Food Chemistry: X 22 (2024) 101336

Contents lists available at ScienceDirect

Food Chemistry: X

journal homepage: www.sciencedirect.com/journal/food-chemistry-x

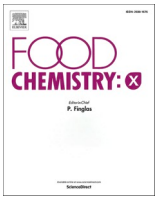

Reusable thiol-modification *Lactobacillus plantarum* embedded in cellulose nanocrystals composite aerogel for efficient removal of Ochratoxin A in grape juice

Mengya Zhao [a,1], Hong Ren [a,1], Zhuomin Yan [a], Jing Ma [a], Xiaoping Feng [a], Di Liu [a], Fangyu Long [a,*]

[a] College of Food Science and Engineering, Northwest A&F University, Yangling, Shaanxi 712100, China

ARTICLE INFO

Keywords:
Thiol-modification *Lactobacillus plantarum*
Cellulose nanocrystals composite aerogel
Ochratoxin A
Grape juice

ABSTRACT

Ochratoxin A (OTA) contamination in grape juice has attracted widespread concern as OTA can lead to kidney disease and cause adverse neurological effects. An effective method to remove OTA is to make use of highly adsorbent materials that are able to remove the toxic contaminant. Recently, inactivated *Lactobacillus plantarum*-based biosorbents have shown to be an efficient, cost-effective and environmentally friendly bioremediation method in removing toxic pollutants such as OTA. We used five chemical thiol-modification methods to improve the adsorption efficiency of OTA in grape juice. The esterification of *Lactobacillus plantarum* (L-Es) significantly increased the sulfhydryl contents (-SH) by 251.33 μmol/g and >90% of OTA was removed. However, the inactivated microbial adsorbent was difficult to separate after adsorption and therefore, the prepared L-Es were embedded into the cellulose nanocrystals (L-Es@CNCs). Moreover, L-Es@CNCs significantly increased the adsorption rate of OTA in grape juice samples by 88.28% with negligible effects on juice quality due to the properties of easy re-use and excellent biodegradability. This showcases its potential application for OTA removal in the grape juice industry.

1. Introduction

Grapes are one of the most popular fruits and make a significant contribution to the economy around the world (Mehri, Esfahani, Heshmati, Jenabi, & Khazaei, 2022; Spinelli et al., 2016). Grape products, especially grape juice, are good sources of organic acids, minerals, phenols, and vitamins (Behfar, Heshmati, Mehri, & Khaneghah, 2022). However, they are extremely susceptible to bruising due to physical collision during transport and are susceptible to fungal infections during cultivation and harvesting (Heshmati, Ghadimi, Ranjbar, & Khaneghah, 2019). Ochratoxin A (OTA) is a secondary metabolite widely present in various foods produced by *Aspergillus* and *Penicillium* fungi, posing a great threat to human health (Schrenk et al., 2020). OTA is a potential safety hazard for grape juice and other grape products because of its genotoxicity, nephrotoxicity, carcinogenicity, teratogenicity, immunosuppression, and hepatotoxicity (Dammak et al., 2022).

OTA is difficult to remove due to the high molecular structure stability and thermal stability (Khoi, Chen, Lin, Chiang, & Hung, 2021). As such, traditional ultraviolet irradiation or ultra-high temperature (UHT) sterilization has a poor effect on OTA removal (Mitchell et al., 2017). Methods for OTA degradation using chemical agents such as acids, chlorides, oxidants, and salt compounds have also been developed. However, this method has certain limitations, including unstable effects, high processing costs, and the use of chemical additives that have a certain impact on the natural flavor of food (Farbo et al., 2016). Therefore, there is an urgent need to develop a method that effectively removes toxins from grape juice, while ensuring its quality. Biosorption mainly utilizes the surface of inactivated microbial cells to bind various fungal toxins (Peng, Meng, Yue, Wang, & Gao, 2021) thereby effectively removing the fungal toxins. Inactivating microorganisms, especially *Lactobacillus plantarum* (*L. plantarum*) have been used to bind with toxins including OTA, zearalenone (ZEN) and patulin (PAT) thereby sequestering them. Other mechanisms of actions include breaking down toxins into less toxic compounds (Li et al., 2023; Li et al., 2023). These applications have generated much attention to their potential use in the removal of toxins in the food industry. Piotrowska (2014) found that L.

* Corresponding author.
E-mail address: fangyu315@126.com (F. Long).
[1] Both authors contributed equally.

https://doi.org/10.1016/j.fochx.2024.101336
Received 18 December 2023; Received in revised form 14 March 2024; Accepted 26 March 2024
Available online 2 April 2024

plantarum LOCK 0862 removed OTA solely using a binding mechanism, adsorbing >80% of total OTA during the first half-hour. The results of Ignacio, Felipe, Carlos, and Verónica (2022) demonstrated that the encapsulation of L. *plantarum* in a polymeric matrix composed of polyvinyl alcohol (PVA) and alginate can be used as a bioremediation method for removing OTA from contaminated wines.

The adsorption capacity of inactivated microorganisms in fruit juice will sharply decrease when applied, most likely due to certain substances in the juice occupying some binding sites (Dallagnol, Bustos, Martos, Valdez, & Gerez, 2019). The adsorption performance of L. *plantarum* can be improved by increasing the number of binding sites (that have high affinity for OTA) through chemical modification. A major disadvantage of inactivating microbial adsorbents is that they are difficult to separate after adsorption. In recent years, the application of polymer adsorbents has received increasing attention because their structures can be synthesized and modified (Huang, Wang, Xue, & Mao, 2018). Aerogel is a special material, which is primarily prepared by removing the liquid solvent in the hydrogel and using gas instead of liquid solvent as the dispersion medium (Ignacio et al., 2022). Nanocellulose is the basic fiber of natural cellulose separated from the aggregation form by chemical, physical, or biological methods (Xu et al., 2021). It has high surface activity, excellent hydrophilicity, mechanical strength, and good biocompatibility (Omran et al., 2021). Nanocellulose is sees as a highly promising material as it combines the advantages of traditional aerogel such as environmental protection, stable chemical properties, simple preparation, and high adsorption with the excellent performance of nanocellulose material (Farbo et al., 2016). As such, the preparation of a convenient and easily separable composite aerogel biosorbent by entrapping inactivated microbial cells in cellulose nanocrystals is likely to be an effective method for OTA control.

In this study, we aimed to evaluate the OTA adsorption effect of thiol-modification L. *plantarum* (L-Es) embedded into the cellulose nanocrystals on grape juice (L-Es@CNCs). The adsorption of OTA by sulfhydryl functional group modification methods of inactivated L. *plantarum* was shown improve adsorption performance. Following this, composite aerogel containing cellulose nanocrystals was prepared and sulfhydryl-modified L. *plantarum* was embedded within. We then established the adsorption kinetics model and isothermal model of L-Es@CNCs for OTA and determined the effects of L-Es@CNCs on the quality of soluble solids, color, and total phenol of grape juice. Our efforts provide a promising application of L-Es@CNCs in the degradation of OTA in grape juice.

2. Materials and methods

2.1. Materials and chemicals

OTA standard, 3-Mercaptopropyltriethoxysilane, N-hydroxysuccinimide, L-cysteine, thioglycolic acid, and microcrystalline cellulose, were purchased from Aladdin (Shanghai, China). *L. plantarum* PA01 was isolated from pickles and registered by the China Common Microbial Collections Management Center (CGMCC No.15660). All chromatographic pure reagents (acetonitrile, methyl alcohol, etc) were purchased from TEDIA (USA). Lipase, Folin-Ciocalteu, and Gallic acid were purchased from Solarbio (Beijing, China). All other annular-grade chemicals (glutaraldehyde, sodium hydroxide, hydrochloric acid, etc) were purchased from Sichuan Xilong Chemical Works (Sichuan, China). Grape juice was provided by Huiyuan Group (Beijing, China) and stored at −20 °C. Grape juice was thawed to room temperature before using.

2.2. Inactivation and thiol modification of L. plantarum

L. plantarum stored at −80 °C was activated three times for fermentation. The activated strain was inoculated into MRS liquid medium according to the inoculation amount of 5% bacterial solution and then placed in a 37 °C shaking table to extend culture for 24 h, and then centrifuged to collect the bacterial sludge (Bayraç & Camızcı, 2019). After washing the bacterial sludge obtained by centrifugation with PBS buffer solution, it was placed in the autoclave, inactivated at 121 °C for 15 min, cooled in the refrigerator at 4 °C, and finally put the pre-cooled bacterial sludge into the freeze dryer for drying.

2.2.1. Silylation modification of L. plantarum

The inactivated L. *plantarum* powder (1.0 g) was washed once with deionized water and three times with 95% ethanol, and then dispersed in 30 mL 95% ethanol. The pH of the cell suspension was adjusted to 4.0 with acetic acid and 1.21 mL (5 mmol) of 3-mercaptopropyltriethoxysilane was added. The mixture was stirred for 24 h, centrifuged at 4 °C, 4000 ×*g* for 5 min for separation, and then lyophilized after washing with ethanol and deionized water (Geng et al., 2017).

2.2.2. Amidation modification of L. plantarum

The inactivated L. *plantarum* powder (1.0 g) was dispersed in 30 mL deionized water. 1-(3-dimethylaminopropyl)-3-ethylcarbodiimide hydrochloride (0.48 g), N-hydroxysuccinimide (0.58 g), 0.606 g (5 mmol) L-cysteine were then added, and the pH of the mixture was adjusted to 7.5 with NaOH, with constant stirring at room temperature for 12 h. The bacterial sludge was then lyophilized after washing with deionized water three times (Qiu et al., 2020).

2.2.3. Esterification modification of L. plantarum

The inactivated L. *plantarum* powder (1.0 g) was dispersed in 20 mL n-hexane, following which 0.345 mL thioglycolic acid and 0.4 g lipase were added. The mixture was stirred at 45 °C for 8 h and then washed with deionized water and lyophilized (Liu, Luo, Wan, Chen, & Wu, 2019; Liu et al., 2019).

2.2.4. Glutaraldehyde crosslinked modification of L. plantarum

The inactivated *L. plantarum* powder (1.0 g) was dispersed in 30 mL deionized water and 0.606 g (5 mmol) L-cysteine was added. The mixture was stirred at room temperature for 2 h and the cells were collected by centrifugation. The L. *plantarum* sludge was then suspended in 40 mL 2.5% (*v*/v) glutaraldehyde solution and stirred at room temperature for 2 h.

2.2.5. Thiourea modification of L. plantarum

1.0 g of *L. plantarum* was added to a 50 mL flask containing 0.38 g thiourea and 20 mL hydrochloric acid. The mixture was stirred at room temperature for 24 h, centrifuged and then washed with deionized water until a value of pH 7.0 was reached. The precipitate was transferred NaOH solution (pH 11.5) and stirred at room temperature for 6 h.

2.3. Characterization and adsorption capacity of thiol-functionalized inactivated microorganisms

We used the Ellman method was used to determine the thiol contents on the surface of L. *plantarum* after thiol modification. Phosphate buffer (0.5 M, pH 8.0, 0.25 mL) and 0.5 mL of 1.6 g/L Ellman solution were mixed for 2 h at room temperature. The mixture was then centrifuged to remove cells, and the absorbance of the supernatant was measured at 450 nm. Sulfhydryl contents were calculated with an L-cysteine calibration curve (Bhatia, Ahuja, & Mehta, 2015). The thiol modified L. *plantarum* were freeze-dried and then ground. Potassium bromide and L. *plantarum* sample were prepared in a ratio of 100:1. The microbial cells were analyzed by Fourier transform infrared (FT-IR, Bruker, Germany) spectroscopy to identify the changes of groups and sulfhydryl groups on the surface of L. *plantarum* cells. A scanning electron microscope (FEI, USA) was used to observe the morphology of the bacterial adsorbent, and the elemental composition and content changes were analyzed by energy-dispersive X-ray photoelectron spectroscopy. The particle size distribution and potential distribution of cellulose nanocrystals (CNCs) were determined by a zeta-sizer instrument (Malvern, England). The

OTA standard was diluted into 0, 50, 100, and 1000 μg/L and stored at −18 °C away from light. The adsorption capacity of bacterial adsorbents in grape juice solution was evaluated based on OTA concentration changes using high-performance liquid chromatography (HPLC, Shimadzu, China) equipped with a fluorescence detector to detect OTA contents (Shukla, Park, & Kim, 2020). The instrument parameter was as follows: column temperature: 30 °C, sample size: 10 μL, flow rate: 1 mL/min, detection (excitation) wavelength: 333 nm, emission wavelength: 460 nm, mobile phases and elution conditions: glacial acetic acid: acetonitrile: water (2 + 99 + 99).

2.4. Preparation of cellulose nanocrystals composite aerogel

The suspension of cellulose nanocrystals (CNCs) with a mass fraction of 4% was prepared, and added dropwise to 5% 3-chloropropyltriethoxysilane (CPTES) to the suspension as the crosslinking agent and stirred at 80 °C for 2 h (Qiu et al., 2020). Subsequently, thiol-functionalized inactivated L. *plantarum* cells were added to the mixed solution, and the amount of thiolated L. *plantarum* powder was adjusted to obtain a series of mixed solutions with different loading amounts of thiolated L. *plantarum* (1 mg/mL, 2 mg/mL, 5 mg/mL, 10 mg/mL, 15 mg/mL and 20 mg/mL). The mixture was then transferred into the wells of the 48-well plate (1.0 cm^2) to form hydrogels. The hydrogels in the plates were frozen at −80 °C for 2 h and then lyophilized to obtain cellulose nanocrystal composite aerogel adsorbents with different thiolated L. *plantarum* loads (Zhang, Elsayed, Navarathna, Schueneman, & Hassan, 2019; Zhang, Yin, Lin, & Kin, 2019).

2.5. Characterization of cellulose nanocrystals composite aerogel

L-Es/CNCs composite aerogel (L-Es@CNCs) with different thiol functionalized L. *plantarum* addition amounts (0 mg/mL, 1 mg/mL, 2 mg/mL, 5 mg/mL, 10 mg/mL, 15 mg/mL and 20 mg/mL) in 30 mg was added to 3 mL of working solution containing 50 μg/L OTA, and then placed in a constant temperature shaker (160 r/min, 25 °C) for 4 h. The adsorption solution was collected using a 0.22 μM filter membrane, and the contents of OTA were then detected by HPLC. The morphology of the L-Es@CNCs was characterized by scanning electron microscopy (SEM) with the acceleration voltage set to 15.0 kV and a working distance of 9.0 mm. The L-Es/CNCs were obtained on the X-ray diffractometer (Tianmei China) using a Ni-filtered Cu-Kα radiation at an anode voltage of 45 kV and 40 mA. Diffractograms were recorded from 5° to 90° at a scan rate of 2° per min.

2.6. Adsorption kinetics models

L-Es@CNCs (30 mg) were added to 3 mL of OTA with an initial concentration of 50 μg/L, 100 μg/L, and 150 μg/L working solution, and then put into a constant temperature shaker (160 r/min, 25 °C) for 0.5, 2, 4, 8, 12, 6, 20, 24 h for the adsorption experiment. The adsorption solution was collected using a 0.22 μM hydrophilic filter membrane filtration. The OTA content was then detected using HPLC and the OTA adsorption capacity was calculated. Experimental data were fitted by the Lagergren pseudo-first-order and pseudo-second-order models to predict the adsorption kinetic of OTA adsorbed by L-Es@CNCs (Bayraç & Camızcı, 2019). The Eq. (1) and (2) are expressed as follows, respectively:

$$Q_t = Q_e \bullet [1 - exp(-k_1 \bullet t)] \quad (1)$$

$$Q_t = \frac{Q_e^{\,2} \bullet k_2 \bullet t}{[k_2] \bullet Q_e \bullet t + 1} \quad (2)$$

where Q_e (μg/g) and Q_t (μg/g) are the amounts of adsorbed OTA on the adsorbent at equilibrium and at time t (h), respectively, and k_1 and k_2 are the adsorption rate constants for the pseudo-first-order adsorption and pseudo-second-order adsorption, respectively.

2.7. Adsorption isotherm models

L-Es@CNCs (30 mg) were added into 3 mL of OTA working solution at three different temperature conditions (25 °C, 35 °C, and 45 °C). The working solution concentrations of OTA were 50, 75, 100, 125, 150, 200, 250, 300, and 400 μg/L, respectively. L-Es@CNCs were then placed in a constant temperature shaker (160 r/min) for a 6 h adsorption test, after which, the adsorption solution was collected using a 0.22 μM filter membrane. The OTA content was then detected using HPLC, and the equilibrium adsorption of OTA was calculated. In order to predict whether the biosorption system is favorable or unfavorable, we discussed the shape of the Langmuir isotherm. The Langmuir model is suitable for monolayer sorption of surfaces with a finite number of identical sites Eq. (3):

$$Q_e = \frac{Q_{max} \bullet K_L \bullet C_e}{1 + K_L \bullet C_e} \quad (3)$$

where Q_e is the adsorbed toxin quantity per gram of biomass at equilibrium (μg/g), and Q_{max} is the maximum specific amount of toxin per gram of biomass corresponding to site saturation (μg/g). C_e is the residual toxin concentration at equilibrium (μg/L). K_L is the Langmuir adsorption constant (L/μg). A plot of C_e/Q_e versus C_e should indicate a straight line of slope $1/Q_{max}$ and intercept of $1/ K_L Q_{max}$.

The Freundlich model supposes that the adsorbent surface is heterogeneous, active sites, and their energy exponential distribution. Experience the Freundlich equation can be written as:

$$Q_e = K_F \bullet C_e^{\,1/n} \quad (4)$$

where K_F and n are the indexes of adsorption capacity and adsorption strength, respectively. K_F is the Freundlich adsorption constant (μg/g)/(μg/L), n is the degree of difficulty of adsorption, C_e is the OTA concentration in the equilibrium state (mg/L), and Q_e is the OTA amount adsorbed per gram of biomass (μg/g).

2.8. Adsorption of cellulose nanocrystals composite aerogel in grape juice

Appropriate amount of standard stock solution was evaporated under nitrogen flow at 45 °C, and then the toxin was dissolved in grape juice to prepare working solutions with different concentrations. L-Es@CNCs (30 mg) were added into 3 mL of grape juice containing OTA 50 μg/L, and the adsorption experiments were carried out in a constant temperature shaker at 25 °C and 160 r/min for 10, 30, 60, 120, 240, and 360 min. Grape juice samples were then collected for OTA extraction and purification. OTA standard residence time was about 11.0 min as per the HPLC chromatogram. The contents of soluble solids in grape juice after OTA adsorption were determined by a handheld refractometer (Yike, China). The pH of grape juice was measured by a pH meter (Weifeng, China) to quantify the effective acidity in grape juice and the color of grape juice was determined using a spectrophotometer (Caipu, China). The Folin phenol method was used to determine the total phenol contents in grape juice after OTA adsorption (Liu, Luo, et al., 2019; Liu, Wang, et al., 2019).

2.9. Statistical analysis

Each experiment was carried out in three independent replicates and all values were expressed as mean values ± standard deviation. Minitab 18.0 was used for one-way ANOVA statistical analysis. A value of $p < 0.05$ was considered statistically significant.

3. Results and discussion

3.1. Comparison of Thiol-modification L. plantarum prepared

3.1.1. The -SH contents and OTA adsorption capacity of thiolated L. plantarum

Inactivated microorganisms are inexpensive and easy to obtain, making them a good method for toxin adsorption (Ge, Xu, Li, Peng, & Pan, 2017; Qiu et al., 2020). Inactivated L. *plantarum* powder was modified with sulfhydryl functional groups by five different methods including silylation (L-Si), amidation (L-Am), esterification (L-Es), glutaraldehyde crosslinked (L-Gl), and thiourea modified (L-Tu) as shown in Fig. 1A. Piotrowska (2014) also found that there is an aggregation reaction between penicillin and sulfhydryl (-SH). Therefore, we speculated that an increase in -SH contents could be beneficial for removing OTA.

All five methods significantly increased the -SH contents on the cell surface as shown in Fig. 1B. The -SH contents of L. *plantarum* were the highest (251.33 μmol/g) in samples modified by esterification reaction (L-Es). Meanwhile, the -SH contents of *L. plantarum* were the lowest (60.01 μmol/g) when modified by thiourea (L-Tu). Qiu et al. (2020) also observed that crosslinking glutaraldehyde significantly increased the -SH contents in yeast cells, and the chemical bond between -SH and patulin played an important role in improving the adsorption capacity. The -SH contents of thiolated L. *plantarum* were different from the Qiu et al. (2020), possibly due to differences between strains, as well as differences in cell wall composition and structure between L. *plantarum* and yeast (Shukla et al., 2020). The four thiol-modification methods were observed to significantly improve the OTA adsorption capacity of L. *plantarum* except for the amidation reaction. The OTA adsorption rates of L. *plantarum* prepared by these treatment methods reached 93.92%, 94.05%, 96.07%, 97.00% (L-Gl, L-Si, L-Tu, L-Es) as shown in Fig. 1C.

The FT-IR spectra showed the unmodified L. *plantarum* and L-Es characteristic absorption band (Fig. 1D). The wide adsorption band of unmodified L. *plantarum* centered at 3301 cm^{-1} could be attributed to O–H/N–H stretching vibration (Omran et al., 2021). The peaks at 1542 cm^{-1} and 1063 cm^{-1} were attributed to N—H bending/C–N stretching vibrations and the C–O–H stretching vibrations, respectively (Mehri et al., 2022). The -SH modified L. *plantarum* after esterification had the -SH stretching vibration peak at 2595 cm^{-1}. The L-Es peak of S—H was weaker due to the aggregation of thiol groups and the binding effect of hydrogen at 2595 cm^{-1} (Bayraç & Camızcı, 2019).

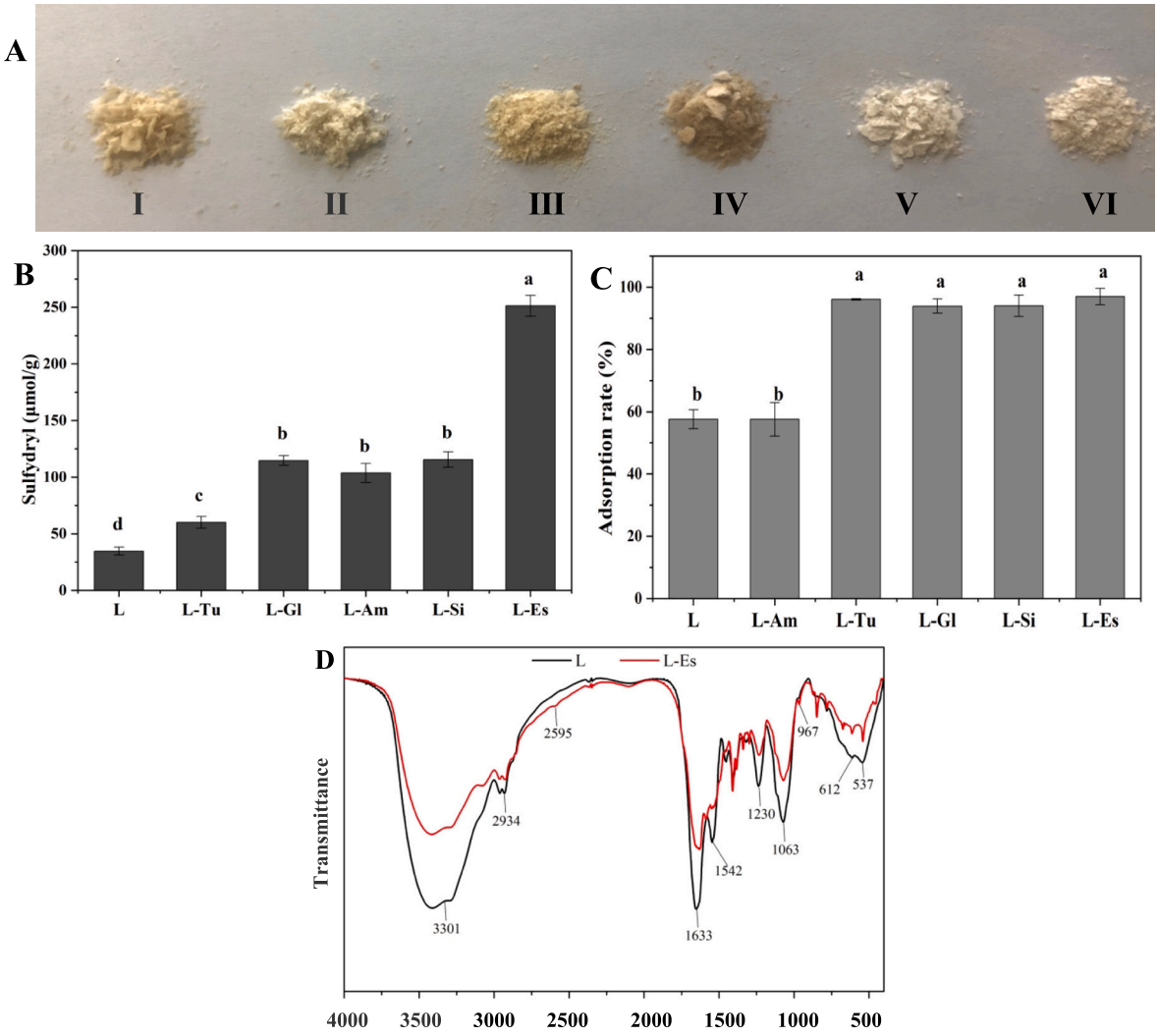

Fig. 1. Preparation and characterization of thiol functionalized inactivated microorganisms. (A) Thiol-modified preparations of L. *plantarum*, L, L-Si, L-Am, L-Es, L-Gl, L-Tu from I to VI. (B) Measurement of -SH contents of L. *plantarum* prepared by different modification methods. (C) OTA adsorption capacity of L. *plantarum* by different modification methods. (D) FT-IR spectrums of L. *plantarum* after esterification modification. The data are shown as means ± SD. Different letters (a, b, c, and d) indicated significant differences between groups ($p < 0.05$).

3.1.2. Scanning electron microscopy energy dispersive spectroscopy (SEM-EDS) of thiol functionalized inactivated L. plantarum

The surface morphologies of thiol-modification L. *plantarum* obtained by esterification are shown in **Fig. S1**. Although the L. *plantarum* surface in the decline phase was slightly ruptured, unmodified L. *plantarum* **(Fig. S1A)** was elliptical with a smooth surface. Esterification modification **(Fig. S1B—D)** results in a rough surface of L. *plantarum* and apparent adhesion between cells, which is likely due to certain adsorption sites being encapsulated internally (Zhang, Elsayed, et al., 2019; Zhang, Yin, et al., 2019). The energy dispersive spectroscopy results showed that the main elements on the cell surface of L. *plantarum* were C, N, and O. As shown in **Fig. S1E,** the elemental image showed the

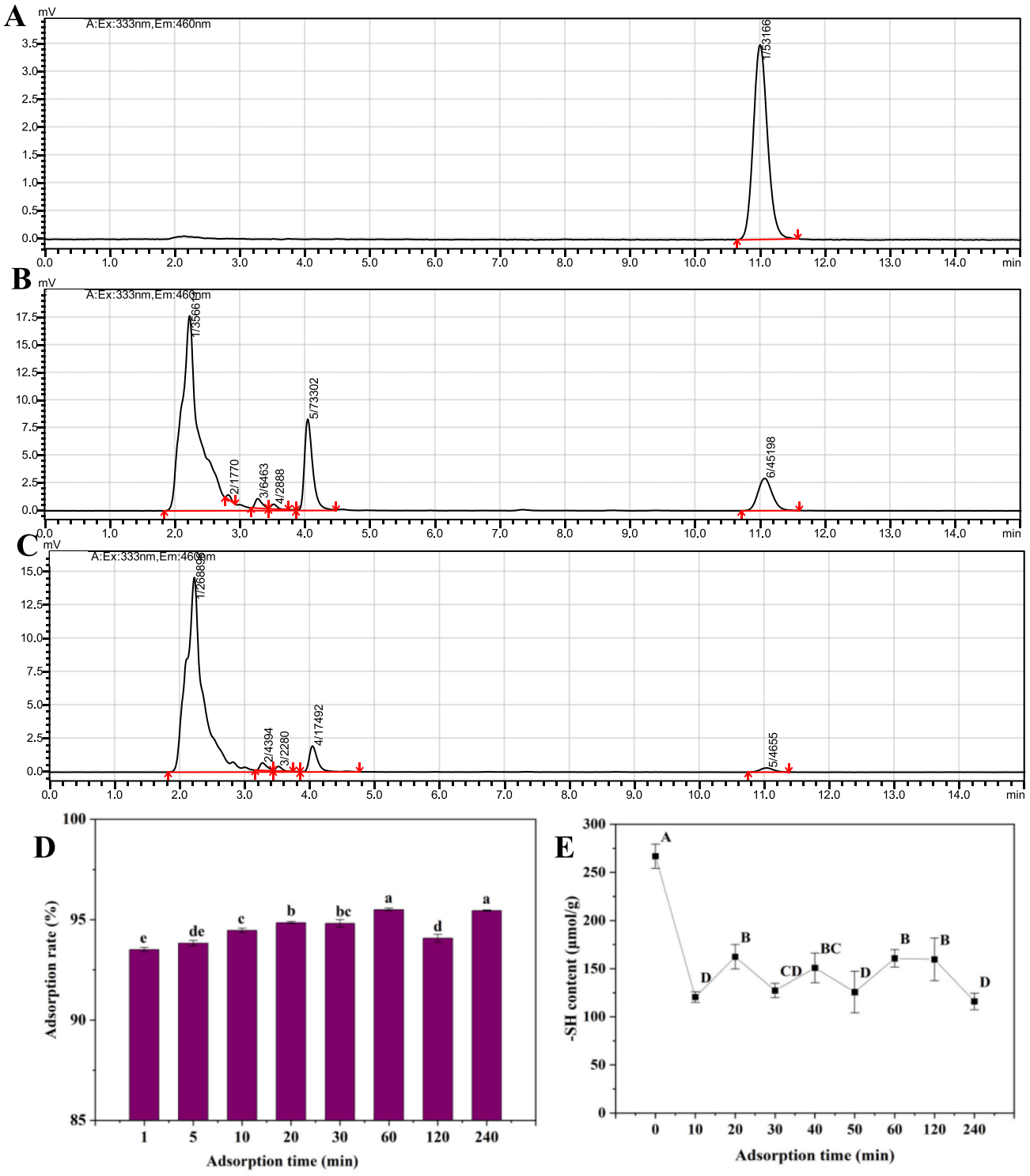

Fig. 2. The adsorption capacity of thiol functionalized inactivated L. *plantarum* to OTA in grape juice. (A) HPLC spectrum of OTA standard. (B) HPLC spectrum of OTA extract from grape juice. (C) HPLC spectrum of OTA extract from grape juice after absorbed by L-Es for 4 h. (D) Adsorption capacity of L-Es to OTA in grape juice. (E) -SH contents of L-Es to OTA adsorption in grape juice. The data are shown as means ± SD. Different letters (a, b, c, d, and e) indicated significant differences between groups ($p < 0.05$).

distribution of sulfur elements in L. *plantarum*, confirming the existence of -SH. In addition, EDS indicated an increase in sulfur elements after thiol-modification, indicating that -SH has been added to the L. *plantarum* **(Fig. S1F)** (Moeinzadeh, Ghadam, Lau, & Emadzadeh, 2019).

3.1.3. Adsorption of OTA by thiol functionalized inactivated microorganisms in grape juice

This study further determined the adsorption efficiency of L-Es on OTA in grape juice, and the results are shown in Fig. 2A-C. As shown in Fig. 2B, the extraction and purification method adopted for OTA from grape juice had better separation efficiency (Shukla et al., 2020). The OTA content in grape juice decreased significantly after 4 h treatment with thiol functionalized inactivated L. *plantarum* adsorbent (Fig. 2C). At the start of adsorption, the -SH contents decreased rapidly, and the corresponding adsorption capacity increased rapidly. The -SH contents of the L-Es fluctuated after 10 min, while the adsorption capacity of the L-Es continued to increase and then reached equilibrium, which was similar to the research conclusion of Liu, Luo, et al. (2019)), Liu, Wang, et al. (2019)). When the adsorption time was 1 min, the adsorption rate of L-Es exceeded 90.0% until equilibrium (95.5%) (Fig. 2D). This suggested that -SH was mainly involved in early adsorption, while other sites on the L. *plantarum* might play a major role in the later stages (Haskard, Binnion, & Ahokas, 2000). The -SH contents decreased to 125 μmol/g after L-Es, and the results showed that the -SH on the surface of L-Es was involved in OTA adsorption (Fig. 2E). This result indicates that the -SH groups on L-Es play a key role in the removal of OTA (Qiu et al., 2020).

3.2. Characterization of L-Es@CNCs and study of adsorbing OTA

3.2.1. Characterization of cellulose nanocrystals

Cellulose nanocrystals (CNCs) were prepared using concentrated sulfuric acid hydrolysis method. This method destroys the amorphous region of cellulose and preserves the crystalline region of cellulose. The CNCs solution system was appeared to be uniformly dispersed and stable **(Fig. S2A)**. The micromorphology of CNCs was observed by transmission electron microscopy (TEM). As shown in **Fig. S2B,** the CNCs show a short rod-shaped morphology, with a length range of about 200–400 nm and a diameter ranging from 20 to 40 nm (Danial et al., 2015). The average size and zeta potential of CNCs were measured by zeta-sizer instrument. The average length of the CNCs was 277.30 nm, while the average width was 39.01 nm, respectively **(Fig. S2C)**. The zeta-sizer instrument used dynamic light scattering in the solution sample to measure size with greater accuracy than transmission electron microscopy (Shaheen & Emam, 2018). Furthermore, the stability of the prepared CNCs was confirmed by monitoring the charge of particles dispersed in solution through zeta potential analysis. The average zeta potential of the CNCs **(Fig. S2D)** was −46.4 mV which confirms that the CNCs are electrically stable due to the attachment of negative sulfate groups to their surface.

The XRD pattern of CNCs had a higher peak at $2\theta = 22.6^{\circ}$ and two weaker diffraction peaks at $2\theta = 14.7^{\circ}$ and $2\theta = 16.8^{\circ}$, which were assigned to the typical spectrogram of cellulose I (**Fig. S2E)**. (Jin et al., 2016). It can be seen from the peak shape that the proportion of amorphous regions in cellulose was small and the crystallinity was high after hydrolysis with concentrated sulfuric acid. The crystallinity of CNCs was 63% calculated by the crystallinity calculation formula. The FT-IR spectra characterization result of CNCs is shown in **Fig. S2F**. The absorbances at 3352 cm^{-1}, 2900 cm^{-1}, 1644 cm^{-1}, 1429 cm^{-1}, 1063 cm^{-1}, 1031 cm^{-1}, 891 cm^{-1} were related to cellulose I, similar to that observed by Tang et al. (2013). A weak absorption peak appeared in the S═O area around 1205 cm^{-1}, which further confirmed the success of esterification (Xu et al., 2021). The strong broad absorption peak appeared -OH stretching vibration peak on the CNCs glucan ring, which indicated that the esterification reaction mainly occurred on the surface and disordered areas of cellulose, with only a small portion occurring inside the crystal structure (Liu, Luo, et al., 2019; Liu, Wang, et al., 2019).

3.2.2. Scanning electron microscope topography analysis

Cellulose nanocrystal composite aerogel was prepared by using 3-chloropropyl triethoxysilane (CPTES) as a crosslinking agent to immobilize L-Es. The influence of different amounts of L-Es on the adsorption capacity of CNCs composite aerogel are shown in **Fig. S3 A**. The adsorption efficiency of composite aerogel on OTA reached about 80% saturation state when the amount of L-Es reached 5 mg/mL. The CNCs composite aerogel obtained by freeze-drying treatment appears to have a good structure **(Fig. S3B)**. Morphological changes of CNCs composite aerogel could be observed from SEM. This weak mechanical response is due to the absence of chemical crosslinking reagents during hydrogel preparation **(**Fig. 3A-B**)** (Zhang, Elsayed, et al., 2019; Zhang, Yin, et al., 2019). The pores of the aerogel increased and the pore size became more uniform after the crosslinking reaction with CPTES **(**Fig. 3C**)**, which indicates the amount of CPTES crosslinking added was appropriate **(**Fig. 3D**)**. As shown in Fig. 3E-F**,** with the addition of L-Es, the aerogel became thicker, but the composite aerogel still maintained a three-dimensional porous structure (Geng et al., 2017).

3.2.3. X-ray diffraction analysis

The XRD spectrum of L-Es added CPTES to the CNCs composite aerogel is shown in **Fig. S4**. The XRD spectrum of all samples exhibited a sharp peak at $2\theta = 22.7^{\circ}$ and two weaker diffraction peaks at $2\theta = 14.7^{\circ}$ and $2\theta = 16.8^{\circ}$, which was consistent with our previous research. Compared with CNCs composite aerogel, the new diffraction peak appeared on the XRD spectrum of CNCs composite aerogel after adding CPTES. The XRD spectrum was the same after adding L-Es, which indicated that L-Es had little effect on the crystal structure of CNCs (Jin et al., 2016).

3.3. Adsorption of OTA by L-Es@CNCs in grape juice

The pH values of adsorption solution were varied from 3.0 to 7.0 to understand the difference in adsorption capacities from a practical view, since most of the liquid foods and grape juice are neutral or slightly acidic (Liu, Luo, et al., 2019; Liu, Wang, et al., 2019). The results **(**Fig. 4A**)** showed that the OTA adsorption rate of L-Es@CNCs significantly decreases with the increase of pH. When the pH increased from 3.0 to 7.0, the OTA adsorption rate decreased from 87.56% to 10.20%, which was similar to the research results of Haskard et al. (2000). The OTA adsorption rate of L-Es@CNCs is not affected in the temperature range of 25–45 °C (Fig. 4B**)**. Higher temperatures are not conducive to OTA adsorption, indicating that adsorption is an exothermic process (Farbo et al., 2016). The reaction time of the interaction between L-Es@CNCs and OTA grape juice samples showed that the adsorption rate of OTA was significantly increased (88.28%) with the reaction time of 4 h **(**Fig. 4C**)**. The results confirmed the efficiency and practicability of the L-Es@CNCs in reducing OTA contents in the actual production of fruit juice drinks (Shukla et al., 2020). The higher initial OTA concentration will increase the collision probability between adsorption weight and adsorption sites. As shown in Fig. 4D, the OTA adsorption rate of L-Es@CNCs was above 80% and increased with the decrease of temperature (Qiu et al., 2020). The OTA adsorption rate begins to decrease gradually when the adsorption system reached the adsorption-desorption equilibrium state.

3.4. Adsorption kinetics and thermodynamic analysis

3.4.1. Adsorption kinetics

The influence of initial concentration of the OTA biological adsorption as shown in Fig. 5A-B. It can be seen that the initial concentration of OTA increased from 50 μg/L to 150 μg/L, and the adsorption capacities of L-Es@CNCs increased significantly from 0 to 13.9 μg/g. The rapid

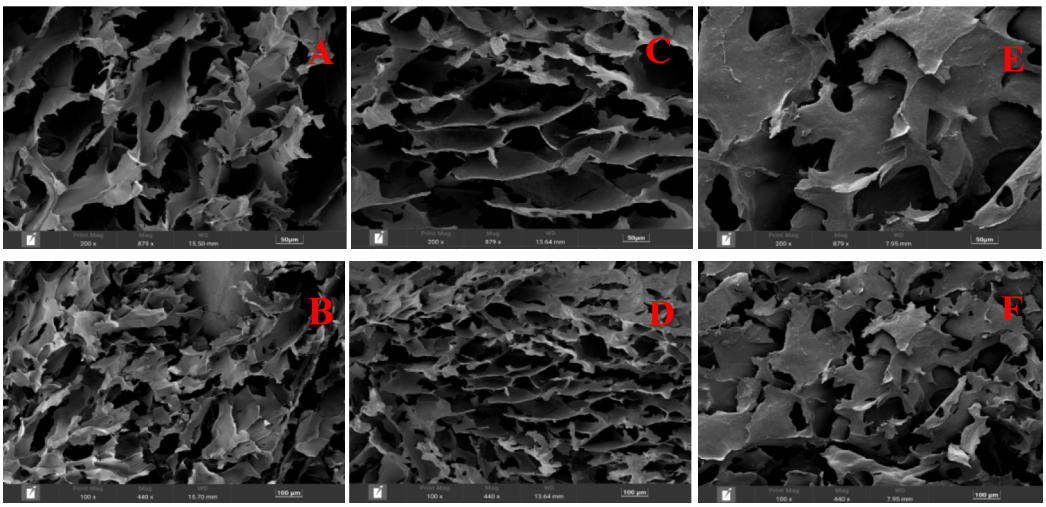

Fig. 3. SEM images of CNCs composite aerogel. (A, B) Pure CNCs composite aerogel. (C, D) CPTES crosslinked CNCs composite aerogel. (E, F) CNCs composite aerogel embedded with L-Es.

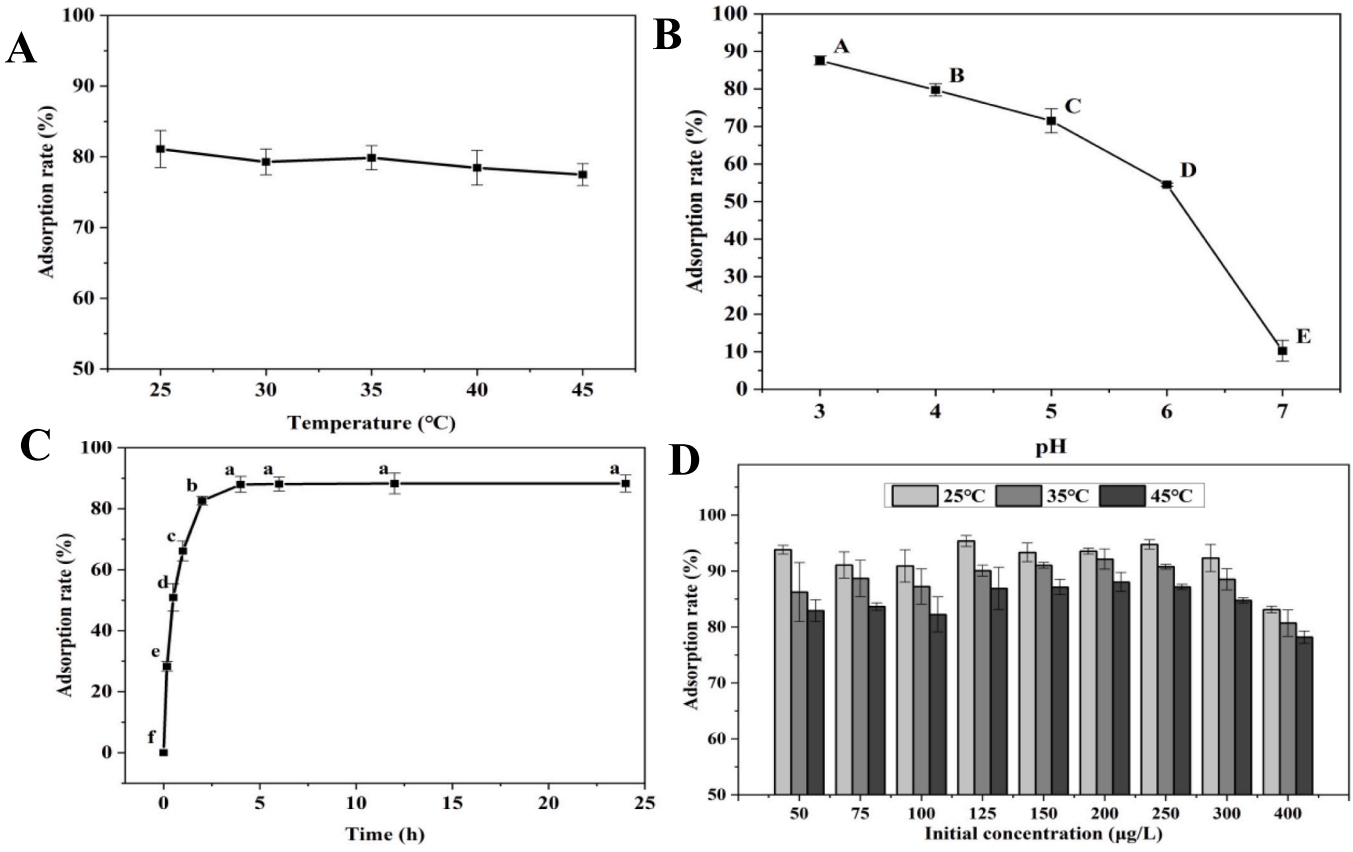

Fig. 4. OTA adsorption capacity of L-Es@CNCs. (A) Effect of pH on OTA adsorption. (B) Effect of temperature on OTA adsorption. (C) Effect of contact time on OTA adsorption. (D) Effect of OTA initial concentration on OTA adsorption capacity. The data are shown as means ± SD. Different letters (a, b, c, d, e, and f) indicated significant differences between groups ($p < 0.05$).

initial adsorption rate gradually stabilized after 5 h. Similar findings were also made by Liu, Luo, et al. (2019)), Liu, Wang, et al. (2019)) of patulin adsorption. The pseudo-first-order kinetic model is based on the assumption that adsorption is controlled by diffusion steps. The pseudo-second-order kinetic model describes that the arrival of adsorbent from the solution to the adsorbent surface is controlled by chemisorption mechanism (Chen et al., 2018). The parameters of the two kinds of dynamic model summary as shown in Table S1. The R^2 of the pseudo-second-order kinetic model was greater than that of the pseudo-first-order kinetic model, and the theoretical adsorption amount (Q_e, cal) calculated by the pseudo-second-order kinetic model was close to the actual adsorption quantities (Q_e, exp) (Bhatia et al., 2015). These results indicated that the pseudo-second-order kinetic model better described the adsorption process than the first second-order model, which further suggests that the covalent bond between -SH and OTA plays a key role in adsorption process (Bhatia et al., 2015).

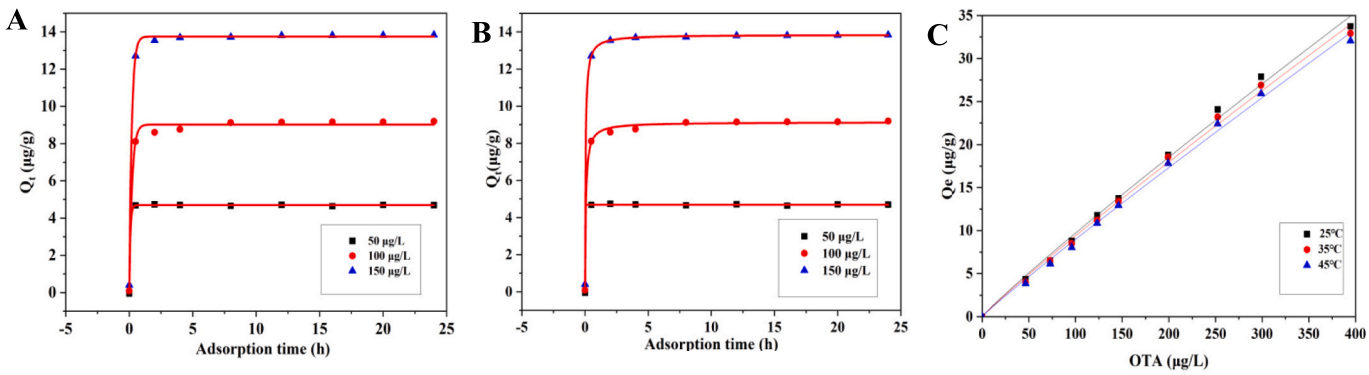

Fig. 5. Adsorption kinetics and isothermal adsorption of L-Es@CNCs adsorption OTA. (A) Pseudo-first-order kinetic equation regression of OTA adsorption on L-Es@CNCs. (B) Pseudo-second-order kinetic equation regression of OTA adsorption on L-Es@CNCs. (C) Adsorption capacity at different initial OTA concentrations.

3.4.2. Adsorption isotherms

Adsorption isotherm refers to the relationship between toxin and adsorption material at a certain temperature when the adsorption process reaches equilibrium between them and the concentration curve (Dallagnol et al., 2019). The Langmuir and Freundlich models are the two most commonly used equations to describe adsorption isotherms in toxin adsorption systems (Farbo et al., 2016). The Langmuir adsorption isotherm describes the adsorption as a monolayer without any other molecular covering layer, whereas the Freundlich isotherm presumes multilayer adsorption processes on an inhomogeneous surface under non-ideal conditions (Ge et al., 2017). As shown in Fig. 5C, the OTA adsorption by L-Es@CNCs was more favorable at 25 °C. The OTA adsorption capacity of L-Es@CNCs significantly increased as the OTA concentration increased from 50 μg/L to 400 μg/L **(**Fig. 5C**)**. Table S2 shown that the adsorption data were more consistent with the Langmuir model with a higher fitting coefficient (R^2). This result suggested that OTA adsorption on the L-Es@CNCs was mainly monolayer adsorption, and the whole adsorption process is mainly chemisorption, similar to results reported by Luo, Li, Yuan, and Yue (2016).

3.5. Effects of L-Es@CNCs treatment on the quality of grape juice

3.5.1. Color changes of grape juice adsorbed by L-Es@CNCs

An important aspect of consumer preference for grape juice is its color. For our experiments, the L-Es@CNCs remained floating in grape juice for 0–24 h. With the extension of adsorption time, grape juice gradually penetrated the interior of the L-Es@CNCs with the structure of L-Es@CNCs remaining intact **(Fig. S5A)**. The state of grape juice remained unchanged during the whole adsorption process, which indicates that the constructed L-Es@CNCs have good adsorption stability and structural stability when added to grape juice. Zhang, Elsayed, et al. (2019)), Zhang, Yin, et al. (2019)) used CPTES as a crosslinking agent to prepare a nanocomposite aerogel based on CNCs for selective oil/water separation. The aerogel floated on the water's surface during the adsorption process, which was consistent with our results.

Because color change is often considered a nutrient concern in juice, we measured the chromaticity change of grape juice after L-Es@CNCs adsorption using a spectrophotometer. We observed a minor color change in the grape juice during the L-Es@CNCs adsorption process **(Fig. S5B)**. The L* value represents the degree of lightness, varying from 0 (black) to 100 (white). The a* value represents the degree of greenness (negative) to redness (positive), and the b* value represents the degree of blueness (negative) to yellowness (positive). With the extension of the adsorption time of L-Es@CNCs, a* and b*of grape juice decreased significantly ($p < 0.05$), while the L* increased significantly ($p < 0.05$). The lower a* and b* value indicates that the grape juice is lighter with fewer red and yellow components, indicating L-Es@CNCs adsorption reduced the Maillard reaction, similar to observations reported by Shukla et al. (2020).

3.5.2. Physicochemical quality changes of grape juice adsorbed by L-Es@CNCs

Soluble solids are used to describe all compounds in liquid or fluid foods that can be dissolved in water. The acidity of grape juice affects its edible quality and taste. The refractometer and pH indicator were used respectively to measure the changes in soluble solids and pH of grape juice during the OTA process of L-Es@CNCs adsorption. There was no significant difference ($p > 0.05$) between the soluble solids and titrable acidity (pH) after adsorption in 0–8 h (Fig. 6A-B). The results of Ge et al. (2017) showed that within 15 h of removing patulin, the added biosorbent had no significant effects on the quality parameters, Brix, Vitamin C, and titratable acidity of grape juice samples, which suggest that the adsorbent used for OTA removal should not have a serious impact on the quality of grape juice. The change of total phenol contents in grape juice during the OTA adsorption process at L-Es@CNCs was measured by ultraviolet spectrophotometer (Fig. 6C). With the extension of adsorption time, the total phenol contents of grape juice gradually decreased, which indicated that some polyphenol compounds may also bind to the L-Es@CNCs, resulting in the loss of polyphenol contents (Liu, Luo, et al., 2019; Liu, Wang, et al., 2019).

4. Conclusion

In summary, *L. plantarum* was prepared by esterification reaction and then embedded in cellulose nanocrystals composite aerogel to successfully remove OTA. The new polymer material has the advantages of reusability and superior OTA adsorption capacity. The adsorption kinetics of the L-Es@CNCs toward OTA conforms to the pseudo-second order model, and the endothermic process was consistent with the Langmuir isotherm model. Moreover, the high OTA removal efficiency of L-Es@CNCs was also achieved in grape juice, and the adsorption process not causing any observable deterioration in juice quality. These findings make the L-Es@CNCs as a useful method in the removal of OTA in the grape juice. The adsorption mechanisms of L-Es@CNCs for OTA remain unclear, and further research is needed to improve the material properties, determine the adsorption mechanism, improve the OTA adsorption rate and apply it in the food industry.

CRediT authorship contribution statement

Mengya Zhao: Writing – review & editing, Writing – original draft, Formal analysis, Data curation. **Hong Ren:** Writing – original draft, Formal analysis, Data curation. **Zhuomin Yan:** Resources, Methodology. **Jing Ma:** Resources, Methodology. **Xiaoping Feng:** Software, Resources. **Di Liu:** Software. **Fangyu Long:** Writing – review & editing, Project administration, Funding acquisition, Conceptualization.

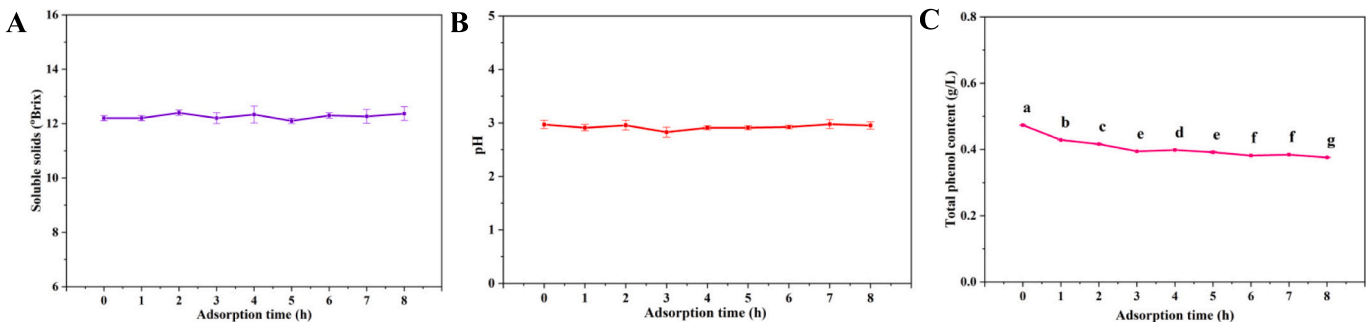

Fig. 6. Changes in physicochemical properties of grape juice after L-Es@CNCs adsorption. (A) Soluble solids contents change of grape juice during adsorption. (B) pH changes of grape juice during adsorption. (C) Total phenol contents change of grape juice during adsorption. The data are shown as means ± SD. Different letters indicated significant differences between groups ($p < 0.05$).

Declaration of competing interest

Authors declare that there are no conflicts of interest.

Data availability

Data will be made available on request.

Acknowledgments

This work was supported by the National Natural Science Fund (No. 31601395), Central Guidance on Local Science and Technology Development Fund of Guizhou Province ([2023] 016), China National Center for Food Safety Risk Assessment (202306).

Appendix A. Supplementary data

Supplementary data to this article can be found online at https://doi.org/10.1016/j.fochx.2024.101336.

References

Bayraç, C., & Camızcı, G. (2019). Adsorptive removal of patulin from apple juice via sulfhydryl-terminated magnetic bead-based separation. *Journal of Hazardous Materials, 366*, 413–422. https://doi.org/10.1016/j.jhazmat.2018.12.001

Behfar, M., Heshmati, A., Mehri, F., & Khaneghah, M. A. (2022). Removal of Ochratoxin a from grape juice by clarification: A response surface methodology study. *Foods, 11*(10), 1432. https://doi.org/10.3390/foods11101432

Bhatia, M., Ahuja, M., & Mehta, H. (2015). Thiol derivatization of Xanthan gum and its evaluation as the mucoadhesive polymer. *Carbohydrate Polymers, 131*, 119–124. https://doi.org/10.1016/j.carbpol.2015.05.049

Chen, Y., Fan, D. B., Lyu, S. Y., Li, G. Y., Jiang, F., & Wang, S. Q. (2018). Elasticity-enhanced and aligned structure nanocellulose foam-like aerogel assembled with cooperation of chemical art and gradient freezing. *ACS Sustainable Chemistry & Engineering, 7*(1), 1381–1388. https://doi.org/10.1021/acssuschemeng.8b05085

Dallagnol, M. A., Bustos, Y. A., Martos, I. G., Valdez, F. G., & Gerez, L. C. (2019). Antifungal and antimycotoxigenic effect of *Lactobacillus plantarum* CRL 778 at different water activity values. *Revista Argentina de Microbiología, 51*(2), 164–169. https://doi.org/10.1016/j.ram.2018.04.004

Dammak, I., Alsaiari, S. N., Fhoula, I., Amari, A., Hamdi, Z., Hassouna, M., & Lasram, S. (2022). Comparative evaluation of the capacity of commercial and autochthonous Saccharomyces cerevisiae strains to remove Ochratoxin a from natural and synthetic grape juices. *Toxins, 14*(7), 465. https://doi.org/10.3390/toxins14070465

Danial, W. H., Majid, Z. A., Muhid, M. N. M., Triwahyono, S., Bakar, M. B., & Ramli, Z. (2015). The reuse of wastepaper for the extraction of cellulose nanocrystals. *Carbohydrate Polymers, 118*, 165–169. https://doi.org/10.1016/j.carbpol.2014.10.072

Farbo, G. M., Urgeghe, P. P., Fiori, S., Marceddu, S., Jaoua, S., & Migheli, Q. (2016). Adsorption of ochratoxin a from grape juice by yeast cells immobilised in calcium alginate beads. *International Journal of Food Microbiology, 217*, 29–34. https://doi.org/10.1016/j.ijfoodmicro.2015.10.012

Ge, N., Xu, J. J., Li, F. L., Peng, B. Z., & Pan, S. Y. (2017). Immobilization of inactivated microbial cells on magnetic Fe_3O_4@CTS nanoparticles for constructing the new biosorbent for removal of patulin in fruit juice. *Food Control, 82*, 83–90. https://doi.org/10.1016/j.foodcont.2017.06.027

Geng, B. Y., Wang, H. Y., Wu, S., Ru, J., Tong, C. C., Chen, Y. F., … Liu, X. Y. (2017). Surface-tailored nanocellulose aerogels with thiol-functional moieties for highly efficient and selective removal of Hg (II) ions from water. *ACS Sustainable Chemistry & Engineering, 5*(12), 11715–11726. https://doi.org/10.1021/acssuschemeng.7b03188

Haskard, C., Binnion, C., & Ahokas, J. (2000). Factors affecting the sequestration of aflatoxin by Lactobacillusrhamnosus strain GG. *Chemico-Biological Interactions, 128*(1), 39–49. https://doi.org/10.1016/S0009-2797(00)00186-1

Heshmati, A., Ghadimi, S., Ranjbar, A., & Khaneghah, M. A. (2019). Changes in aflatoxins contents during processing of pekmez as the traditional product of grape. *LWT - Food Science and Technology, 103*, 178–185. https://doi.org/10.1016/j.lwt.2019.01.001

Huang, W. C., Wang, W., Xue, C. H., & Mao, X. Z. (2018). Effective enzyme immobilization onto the magnetic chitin nanofiber composite. *ACS Sustainable Chemistry & Engineering, 6*(7), 8118–8124. https://doi.org/10.1021/acssuschemeng.8b01150

Ignacio, R. C., Felipe, V. L., Carlos, P., & Verónica, S. C. (2022). Removal of Ochratoxin A from Red Wine Using Alginate-PVA-L. plantarum (APLP) Complexes: A Preliminary Study. *Toxins, 14*(4), 230. https://doi.org/10.3390/TOXINS14040230

Jin, E. S., Guo, J. Q., Yang, F., Zhu, Y. Y., Song, J. L., Jin, Y. C., & Rojas, J. O. (2016). On the polymorphic and morphological changes of cellulose nanocrystals (CNC-I) upon mercerization and conversion to CNC-II. *Carbohydrate Polymers, 143*, 327–335. https://doi.org/10.1016/j.carbpol.2016.01.048

Khoi, C. S., Chen, J. H., Lin, T. Y., Chiang, C. K., & Hung, K. Y. (2021). Ochratoxin A-induced nephrotoxicity: Up-to-date evidence. *International Journal of Molecular Sciences, 22*(20), Article 11237. https://doi.org/10.3390/ijms222011237

Li, Q. Q., Zeng, X. Q., Fu, H. L., Wang, X. M., Guo, X. J., & Wang, M. (2023). Lactiplantibacillus plantarum: A comprehensive review of its antifungal and anti-mycotoxic effects. *Trends in Food Science and Technology*. https://doi.org/10.1016/j.tifs.2023.04.019

Li, Y. C., Yang, L., Lu, Y. S., Wang, M. M., Liu, M. J., & Wang, S. (2023). Coupled adsorption and photocatalysis: A green synthesized g-C_3N_4@Mn–FeOOH@ molecularly imprinted photocatalysis system for targeted removal of various heterocyclic amines. *Food Frontiers, 1-14*. https://doi.org/10.1002/fft2.316

Liu, L. F., Luo, J. Q., Wan, Y. H., Chen, X. R., & Wu, Y. P. (2019). Mussel-inspired membrane adsorber with thiol ligand for patulin removal: Adsorption and regeneration behaviors. *Macromolecular Materials and Engineering, 304*(6), Article 1800790. https://doi.org/10.1002/mame.201800790

Liu, M. S., Wang, J., Wang, X., Zhu, W. X., Yao, X. L., Su, L. H., … Wang, J. L. (2019). Highly efficient and cost-effective removal of patulin from apple juice by surface engineering of diatomite with sulfur-functionalized graphene oxide. *Food Chemistry, 300*, Article 125111. https://doi.org/10.1016/j.foodchem.2019.125111

Luo, Y., Li, Z., Yuan, Y. H., & Yue, T. L. (2016). Bioadsorption of patulin from kiwi fruit juice onto a superior magnetic chitosan. *Journal of Alloys and Compounds, 667*, 101–108. https://doi.org/10.1016/j.jallcom.2016.01.143

Mehri, F., Esfahani, M., Heshmati, A., Jenabi, E., & Khazaei, S. (2022). The prevalence of Ochratoxin A in dried grapes and grape-derived products: The systematic review and meta-analysis. *Toxin Reviews, 41*(1), 347–356. https://doi.org/10.1080/15569543.2020.1845739

Mitchell, J. N., Chen, C., Palumbo, D. J., Bianchini, A., Cappozzo, J., Stratton, J., & Wu, F. (2017). A risk assessment of dietary Ochratoxin the in the United States. *Food and Chemical Toxicology, 100*, 265–273. https://doi.org/10.1016/j.fct.2016.12.037

Moeinzadeh, R., Ghadam, G. J. A., Lau, W. J., & Emadzadeh, D. (2019). Synthesis of nanocomposite membrane incorporated with amino-functionalized cellulose nanocrystals for refinery wastewater treatment. *Carbohydrate Polymers, 225*, Article 115212. https://doi.org/10.1016/j.carbpol.2019.115212

Omran, B. A. A., Mohammed, A. A., Sapuan, M. S., Ilyas, A. R., Asyraf, M. R. M., Rahimian Koloor, S. S., & Petrů, M. (2021). Micro-and nanocellulose in polymer composite materials: A review. *Polymers, 13*(2), 231. https://doi.org/10.3390/polym13020231

Peng, W. Y., Meng, D. Q., Yue, T. L., Wang, Z. L., & Gao, Z. P. (2021). Effect of the apple cultivar on cloudy apple juice fermented by the mixture of *Lactobacillus acidophilus*, *Lactobacillus plantarum*, and *Lactobacillus fermentum*. *Food Chemistry, 340*, Article 127922. https://doi.org/10.1016/j.foodchem.2020.127922

Piotrowska, M. (2014). The adsorption of Ochratoxin A by Lactobacillus species. *Toxins, 6*(9), 2826–2839. https://doi.org/10.3390/toxins6092826

Qiu, Y., Zhang, Y. X., Wei, J. P., Gu, Y. G., Yue, T. L., & Yuan, Y. H. (2020). Thiol-functionalized inactivated yeast embedded in agar aerogel for highly efficient

adsorption of patulin in apple juice. *Journal of Hazardous Materials, 388*, Article 121802. https://doi.org/10.1016/j.jhazmat.2019.121802

Schrenk, D., Bodin, L., Chipman, K. J., Mazo, J., Grasl-Kraupp, B., Hogstrand, C., & Bignami, M. (2020). Risk assessment of ochratoxin A in food. *EFSA Journal, 18*, 107–115. https://doi.org/10.2903/j.efsa.2020.6113

Shaheen, T. I., & Emam, H. E. (2018). Sono-chemical synthesis of cellulose nanocrystals from wood sawdust using acid hydrolysis. *International Journal of Biological Macromolecules, 107*, 1599–1606. https://doi.org/10.1016/j.ijbiomac.2017.10.028

Shukla, S., Park, H. J., & Kim, M. (2020). Efficient, safe, renewable, and industrially feasible strategy employing Bacillus subtilis with alginate bead composite for the reduction of ochratoxin A from wine. *Journal of Cleaner Production, 242*, Article 118344. https://doi.org/10.1016/j.jclepro.2019.118344

Spinelli, R. F., Dutra, V. S., Carnieli, G., Leonardelli, S., Drehmer, P. A., & Vanderlinde, R. (2016). Detection of addition of apple juice in purple grape juice. *Food Control, 69*, 1–4. https://doi.org/10.1016/j.foodcont.2016.04.005

Tang, R. L., Huang, B., Lu, L. Q., Wang, Q. S., Ou, W., Lin, Y. W., & Chen, R. X. (2013). Ultrasonication-assisted manufacture of cellulose nanocrystals esterified with acetic acid. *Bioresource Technology, 127*, 100–105. https://doi.org/10.1016/j.biortech.2012.09.133

Xu, T., Du, H. S., Liu, H. Y., Liu, W., Zhang, X. Y., Si, C. L., & Zhang, K. (2021). Advanced nanocellulose-based composites for flexible functional energy storage devices. *Advanced Materials, 33*(48), Article 2101368. https://doi.org/10.1002/adma.202101368

Zhang, X., Elsayed, I., Navarathna, C., Schueneman, T. G., & Hassan, B. E. (2019). Biohybrid hydrogel and aerogel from self-assembled nanocellulose and nanochitin as the high-efficiency adsorbent for water purification. *ACS Applied Materials & Interfaces, 11*(50), 46714–46725. https://doi.org/10.1021/acsami.9b15139

Zhang, Y., Yin, M. L., Lin, X. H., & Kin, S. I. (2019). Functional nanocomposite aerogels based on nanocrystalline cellulose for selective oil/water separation and antibacterial applications. *Chemical Engineering Journal, 371*, 306–313. https://doi.org/10.1016/j.cej.2019.04.075